Strong pinning effect and magnetic nanodomain formation by coupling between magnetic and crystallographic domains in the ordered double perovskite Ba$_2$FeMoO$_6$

T. Asaka,[1] X. Z. Yu,[1,2] Y. Tomioka,[3] Y. Kaneko,[2] T. Nagai,[4] K. Kimoto,[1,4] K. Ishizuka,[5] Y. Tokura,[2,3,6] and Y. Matsui[1,4]

[1]*Advanced Nano Characterization Center (ANCC), National Institute for Materials Science (NIMS), Tsukuba 305-0044, Japan*

[2]*Spin Superstructure Project, Exploratory Research for Advanced Technology (ERATO), Japan Science and Technology Agency (JST),*
Tsukuba 305-8562, Japan

[3]*Correlated Electron Research Center (CERC), National Institute of Advanced Industrial Science and Technology (AIST),*
Tsukuba 305-0046, Japan

[4]*High-Voltage Electron Microscopy Station (HVEMS), National Institute for Materials Science (NIMS), Tsukuba 305-0044, Japan*

[5]*HREM Research, Inc., Matsukazedai, Saitama 355-0055, Japan*

[6]*Department of Applied Physics, University of Tokyo, Tokyo 113-8656, Japan*

We investigated relations between magnetic and crystallographic domains in a single crystal of an ordered double perovskite, Ba$_2$FeMoO$_6$, by means of transmission electron microscopy. By direct observation of the magnetic domain and antiphase domain structures, we demonstrated that magnetic domain walls perfectly coincide with crystallographic antiphase domain boundaries. In addition, we observed a change of magnetic domain structures by applying magnetic fields. Most of the magnetic domains undergo the rotation so as to be along the applying fields, while the local regions with magnetization direction opposite to the applying field remain adjacent to the antiphase boundary. This suggests a strong pinning effect on the magnetic domains at the antiphase boundaries. Moreover, we successfully observed a magnetic nanodomain structure derived from coupling between magnetic and structural ordering domains where Fe/Mo short-range ordering was developed. We found that the magnetic domain structure in the ordered double perovskite is significantly affected by the crystallographic structures, i.e., the antiphase boundary and the short-range ordering, due to their strong mutual coupling.

PACS number(s): 75.60.Ch, 75.50.Gg, 61.72.Ff, 75.70.Kw

I. INTRODUCTION

Ordered double perovskites, AE_2FeMoO$_6$ (AE=Ca, Sr, and Ba), have attracted considerable attention because of their unusual electrical and magnetic properties, such as intergrain-tunneling-type magnetoresistance, half metallic electronic structure, and high Curie temperature (T_C).[1] In AE_2FeMoO$_6$, two different ions, Fe^{3+} and Mo^{5+}, are ordered at the B site of the perovskite structure in a manner of rocksalt-type structure, as illustrated in Fig. 1(a).[2] In the localized-spin model, magnetic interaction between Fe^{3+} (S =5/2) and Mo^{5+} (S=1/2) ions is antiferromagnetic in nature, leading to a ferrimagnetic ground state.[3] However, the localized-spin model cannot explain some of the physical properties in AE_2FeMoO$_6$, such as the metallic conductivity below T_C,[1,4] and the noninteger valence of Fe,[5–9] although neutron diffraction,[10,11] nuclear magnetic resonance,[12] and x-ray magnetic circular dichroism[13] studies have shown experimental evidences of the ferrimagnetic spin arrangement. Recently, the magnetism in AE_2FeMoO$_6$ has been interpreted by indirect Fe-O-Mo-O-Fe exchange interaction mediated itinerant electrons.[1,14] As an intuitive picture of this model, up spins in the Fe sublattice are localized, while the magnetism in the Mo sublattice is borne by itinerant electrons with down spins. This model is supported by the positive exchange Curie-Weiss constant measured in the paramagnetic regime, which suggests that the nearest-neighbor magnetic interaction is ferromagnetic in nature.[15] Besides, actual compounds intrinsically contain antisite defects and antiphase-domain (APD) structures. In the former, Mo^{5+} sites are locally occupied by Fe^{3+} ions and vice versa. The latter is caused by a spatial distribution of the Fe/Mo-ordering domains and out-of-phase ordering. In other words, we can regard a boundary between APDs, i.e., an antiphase boundary (APB), as a "planar" antisite defect. Defect structures locally interrupt the original ferrimagnetic coupling between Fe^{3+} and Mo^{5+} ions or the indirect Fe-O-Mo-O-Fe exchange interaction. This reduces the saturation magnetizations of the ordered double perovskites.[1,16,17] Furthermore, the magnetoresistivities observed in the single crystal[4] and the single-crystalline films[18] (i.e., grain-boundary-free samples) are probably due to antisite defects or APBs.

The APB is likely to affect the magnetic domain (MD) structures. Figure 1(b) displays a schematic illustration of the APB viewed along the [$\bar{1}$10]-zone axis. This shows that the ordering configuration shifts by $\frac{1}{2}d(111)$ across the APB [$\frac{1}{2}d(111)$-type APB]. Strong antiferromagnetic Fe-O-Fe interactions across the APB would orient magnetic moments of neighboring APDs in antiparallel directions.[19] In other words, it is expected that the interactions between the APD and local magnetic moments produce magnetic domain walls (MDWs) on the APB. The observations of the APB have been done using Mössbauer spectroscopy[7,20] or transmission electron microscopy.[21,22] Yu *et al.* have directly observed the pinning effect of the MDWs at the APBs in Ba$_2$FeMoO$_6$ using high-resolution transmission electron microscopy (HR-TEM) and dark-field (DF) imaging to observe the APDs, and Lorentz transmission electron microscopy (LTEM) to observe the MDs.[23] Here, we report more detailed research in the interaction between the crystallographic APD and MD structures for a double perovskite with combined use of the DF imaging, and the LTEM as well as semiquantitative
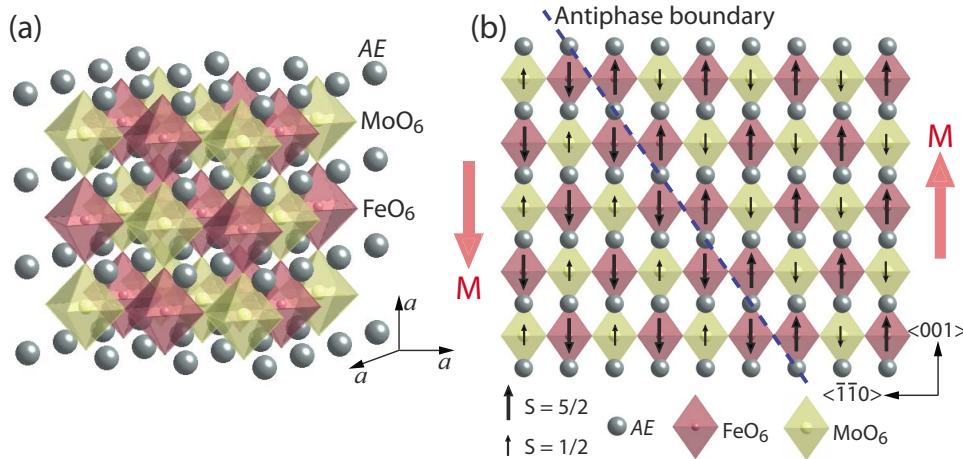
FIG. 1. (Color online) (a) Schematic representation of crystal structure of $AE_2\text{FeMoO}_6$ and (b) representation of antiphase boundary in the $(\bar{1}10)$ plane. The spin arrangement in (b) is based on the localized-spin model. The large arrows denote magnetizations in each ferrimagnetic domain. The dashed line indicates an antiphase boundary, where the localized magnetic moments exhibit an antiferromagnetic coupling.

analysis of local magnetization. We demonstrate a strong pinning effect on the MD at the APB by careful analyses of the domain structures and *in situ* observation under external magnetic fields. A magnetic nanodomain structure in the region where Fe/Mo short-range ordering is developed is presented in this study. To the best of our knowledge, this is the first direct observation of the magnetic nanodomain structure which is derived from coupling between magnetic and structural ordering domains.

II. EXPERIMENTS

To avoid the complexity in analyses of LTEM images due to grain and crystallographic twin boundaries, we adopted a single crystal of $\text{Ba}_2\text{FeMoO}_6$, which has a cubic structure with $a_0 = 0.808$ nm $\approx 2a_p$ ($a_p \approx 0.39$ nm: the lattice constant of simple cubic perovskite),[24–26] for our TEM observation. A single crystal of $\text{Ba}_2\text{FeMoO}_6$ was grown by a floating-zone method, as described in detail in Ref. 4. This crystal has the T_C of ~ 330 K and the saturation magnetization (M_s) of $\sim 2.9\mu_B$/formula unit at 5 K, which is relatively low compared to the ideal value ($4\mu_B$/formula unit).[23] For the TEM observation, the crystal was thinned by mechanical grinding and an Ar^+ ion sputtering. The specimen thickness in the observed area was ~ 150 nm or less. The specimens were warmed at temperatures between room temperature and 336 K and were examined using a Lorentz electron microscope, Hitachi HF-3000L, which is equipped with a custom-made field-free objective lens as well as an external magnetic-field generator to apply magnetic field horizontally to the sample. Using this generator, we carried out *in situ* observation of the change of MD structure under magnetic fields. We applied magnetic fields up to 80 Oe for the *in situ* observation. We used the conventional Fresnel method for magnetic domain imaging, and analyzed the Fresnel images using the commercial software QPT FOR DIGITALMICROGRAPH,[27] which enabled us to quantitatively measure the phase changes of electron waves and the local magnetization in the sample, based on the transport-of-intensity equation (TIE).[28–30] The three Fresnel images taken under different defocus conditions, i.e., underfocused, in-focus, and overfocused, were utilized as input data.

III. RESULTS AND DISCUSSION

Figure 2 displays the results indicating a close coupling between APD and MD. All the electron micrographs were obtained in the same area of the crystal oriented along the $[\bar{1}10]$-zone axis. This projection is the same as in Fig. 1(b), which illustrates APB. Figure 2(a) shows a Fresnel image of $\text{Ba}_2\text{FeMoO}_6$ at room temperature. Dark and bright lines are divergent and convergent images, respectively, corresponding to MDWs. The MDWs were found to intermittently develop perpendicularly to the [111] direction. Figure 2(b) shows the local magnetization distribution map calculated with the TIE method. The inset of Fig. 2(b) is a color wheel for interpretation of the color distribution map. In the color wheel, color phase and brightness represent the direction and magnitude of magnetization, respectively. Thus regions with homogeneous colors and boundaries with abrupt changes in color phases in Fig. 2(b) represent MDs and MDWs, respectively. The MDs are an irregular shape on a submicrometer scale. In conventional single-crystalline ferromagnets, magnetic domains are uniform and show a regular array. In this respect, the observed MD structure of $\text{Ba}_2\text{FeMoO}_6$ is unique. Figure 2(c) shows a dark-field image with use of the 111 spot [marked as a white circle in Fig. 2(a)]. Dark lines or areas represent the APBs. The width of the dark line does not indicate the intrinsic width of the APB. The sharp lines indicate that the incident beam is nearly parallel to the APB, in the so-called "edge-on condition," while the broad lines and even the dark areas also indicate the APB. Broadening of the boundary image is due to deviation from the edge-on condition. Most of the observed APBs are $\frac{1}{2}d(111)$-type ones. We observed bending and branching of the MDW in the Fresnel images due to the intricate APD structure. Moreover, the MDWs coincide with the APBs in most parts of the observed area, as shown in Figs. 2(b) and 2(c). Arrows in Fig. 2(c) represent the local magnetization distribution obtained by the TIE method. Most of the MDWs are 180° ones. The local magnetization directions were found to be almost perpendicular to the [111] direction. Namely, the magnetic moments were roughly along the APB. We found that the MD corresponds one-to-one with the APD in most parts of the crystal. This also means that the MDWs are strongly pinned at APBs. We conclude that the irregular shape of the observed MDs is
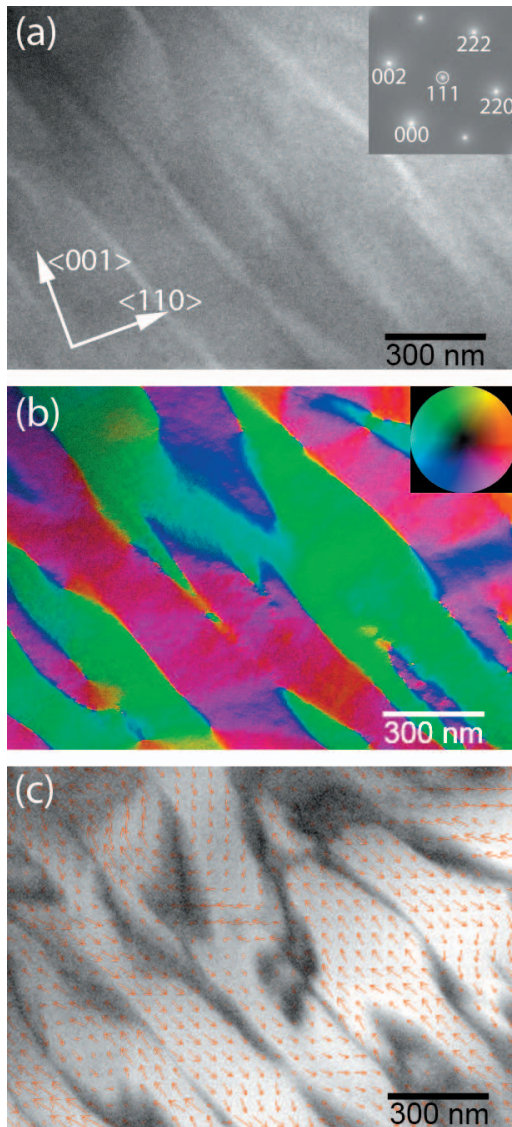
FIG. 2. (Color) Magnetic and antiphase domain structures in Ba_2FeMoO_6. (a) The $[\bar{1}10]$-zone Fresnel image. The bright and dark lines represent magnetic domain walls. The inset is the corresponding electron diffraction pattern. (b) Magnetization-distribution map derived by the transport-of-intensity equation (TIE) method. The inset is a color wheel for interpretation of the color distribution map. (c) The $[\bar{1}10]$-zone dark-field image formed with the 111 spot. Dark lines and areas indicate the antiphase boundaries. The small red arrows represent local magnetization.

due to this pinning effect. Such interaction between APBs and MDWs has previously been observed in other materials having structural order, such as metallic alloys[31–33] and Fe_3O_4 film.[34] In particular, a one-to-one correspondence of MDWs and APDs has been observed in Heusler alloy, Cu_2MnAl, where the pinning might be ascribed to antiferromagnetic coupling at the APB.[32] As mentioned above, the APBs in AE_2FeMoO_6 is also likely to be antiferromagnetic. We assigned the observed pinning effect to the antiferromagnetic coupling at the APB.

To better understand the nature of the coupling between the APB and the MDW, we measured widths of MDWs and compared them with the projections of APBs in the DF images. The widths of the divergent and convergent images of MDWs do not correspond to intrinsic MDW widths, because they were obtained under an out-of-focus condition. There are several known methods to measure the MDW width by LTEM imaging. We used the Wade's method[35] in which the MDW width δ was derived by measuring the widths of the divergent or convergent images in several Fresnel images that were obtained by changing the defocus distance z. In Wade's method, the formula for the MDW width in the divergent image is

$$W_d(z) = \delta_0 + 2z\Psi,$$

where Ψ is the deflection angle of outgoing electrons due to the Lorentz force depending on local magnetization. Here $W_d(z)$ is the full width at half maximum (FWHM) for the intensity profiles across the MDW divergence images. The value δ_0, i.e., the MDW width, can be derived from a linear asymptote $W_d(0) = \delta_0$ at zero defocus $(z=0)$.[35,36] [Note that we cannot obtain MDW images under zero defocus (in-focus condition) in the Fresnel method.]

To compare the APB and the MDW, we discuss not the intrinsic APB and MDW widths but their projections onto the two-dimensional observation plane, because the edge-on conditions for the APB and the MDW were not always realized. In the areas where the dark-line contrasts from APBs were observed in the DF images, sets of Fresnel images whose defocus distances changed were obtained. The tilting angle of the specimen was maintained during the DF and Fresnel observations for one set of APB and MDW. One example of this experimental procedure is shown in Fig. 3. Figure 3(a) is the DF image showing the dark-line contrast from the APB, while Fig. 3(b) is the Fresnel image showing the divergent image from MDW. Figure 3(c) shows the image-intensity profiles across the dark-line contrasts from the APB and MDW, as indicated by the lines in Figs. 3(a) and 3(b). The dashed curves in Fig. 3(c) represent the resultant profiles of Gaussian fitting for the respective intensity profiles. For the Fresnel observation, we obtained the three to five different defocused images. We measured the full width at half maximum (FWHM) for the intensity profiles (the Gaussian fitted profiles) of the APB and MDW. For the MDW, we estimated the width of the projection image of MDW by extrapolating the FWHM for $W_d(z)$ from defocus to in focus $(z=0)$, while we regarded the measured FWHM as the width of the projection image of the APB. Figure 3(d) plots the FWHM of the width of the MDW divergent images for the area shown in Fig. 3(b) as a function of the defocus distance. Based on the best-fit linear function (derived by the least-square method), the width of the projection image of MDW, δ_0, was estimated at $\sim$33 nm. We plotted in Fig. 3(e) the widths of the projection images of MDWs obtained by this means as a function of the width of the APB projection image. As shown in Fig. 3(e), the width of the MDW projection image increases almost linearly with the width of the APB projection image. This strongly suggests that the MDW perfectly coincides with the APB, even in the depth direction along the electron beam.
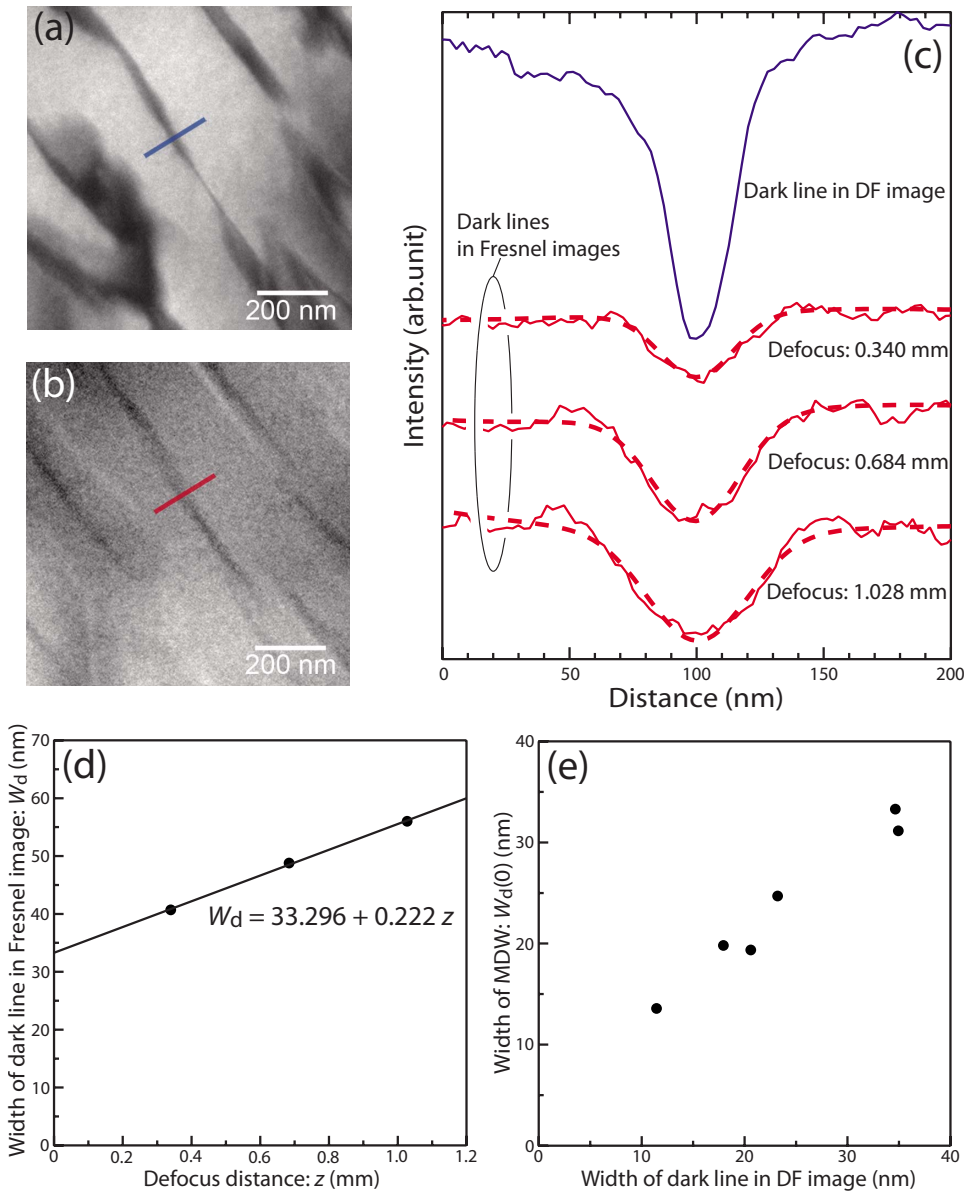
FIG. 3. (Color online) Relations between widths of magnetic domain walls and antiphase domain boundary. (a) The dark-field image and (b) the Fresnel image. (c) Profiles of image intensities of regions indicated by lines in (a) and (b). The solid and dashed curves denote raw and Gaussian fitted data. (d) The width (FWHM) of the MDW divergent image as a function of the defocus distance. The width of the MDW was derived by extrapolating $W_d(z)$ from defocus to in focus ($z=0$). (e) The width of the MDW as a function of the width of the dark line representing APB in the dark-field image.

We display in Fig. 4 the variation of MD structures under external magnetic fields H. The magnetic fields were applied along the (111) plane (i.e., along most of the APBs). With applying magnetic field of 20 Oe, we observed rotation of local magnetization directions to be along H, as shown in Fig. 4(h). With increasing applying field, rotation of magnetization directions was observed in the domains where originally ($H=0$) the magnetization directions opposite to the applying field. Namely, nucleation of new domains having local magnetization direction along H was discerned, as shown in Fig. 4(j). Upon further increasing H to 80 Oe, the magnetization directions were almost along H in most parts of the sample, while the domains having the magnetization directions almost opposite to the applying field remained locally. Comparing with the dark-field image shown in Fig. 4(f), we can recognize that only the regions adjacent to the APB exhibited the local magnetization direction opposite to the applying field. Such a behavior of the MDs under the external magnetic fields also indicates the pinning effect of the MD at the APB.

We observed the strong coupling between crystallographic domains and MDs, in a region with short-range Fe/Mo ordering. By Fresnel imaging, we observed characteristic granular contrast as well as the MDW contrast. The granular contrast is displayed on the right in Fig. 5(a), while the MDW contrast is on the left. The broad curved black lines are bend contours. Figures 5(a)–5(d) and 5(f) show the temperature profiles of the Fresnel images. On heating from 300 K, the MDW images and the granular contrasts gradually decreased and eventually vanished above ~330 K, i.e., close to T_C [Figs. 5(e) and 5(f)]. The behaviors of the MD and granular structures during the cooling process from above T_C were similar to those during the heating process. These suggest that the granular contrast is attributable to the magnetic objects. Figure 5(g) shows the magnified Fresnel image of the granular contrast. Indistinct granular structure with 10–30-nm diameters was found. Figure 5(h) is the TIE image corresponding to the region shown in Fig. 5(g). Homogeneously colored areas in Fig. 5(h) represent magnetic nanodomains, which appear intricately tangled.
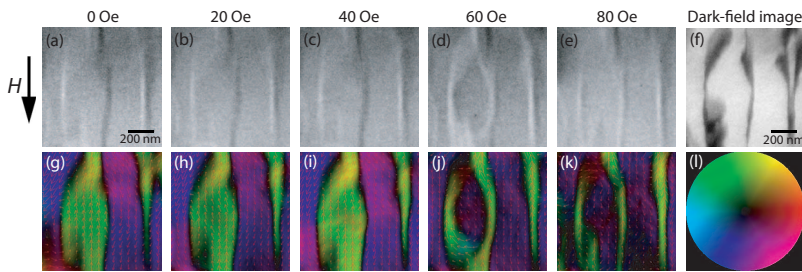
FIG. 4. (Color) External magnetic-field profiles of magnetic domain structures. The Fresnel images under the magnetic fields of (a) 0, (b) 20, (c) 40, (d) 60, and (e) 80 Oe. (f) The dark-field image formed with the 111 spot at the same area. The panels (g)–(k) are the TIE images corresponding to (a)–(e), respectively. Arrows represent local magnetization. (l) The color wheel for interpretation of the color distribution map.

Figure 5(i) shows the intensity profiles of the 111 diffraction spot arising from the Fe/Mo ordering for the granular contrast area (blue line) and the MDW contrast area (red line). Obviously, the diffraction spots with hkl, where h, k,
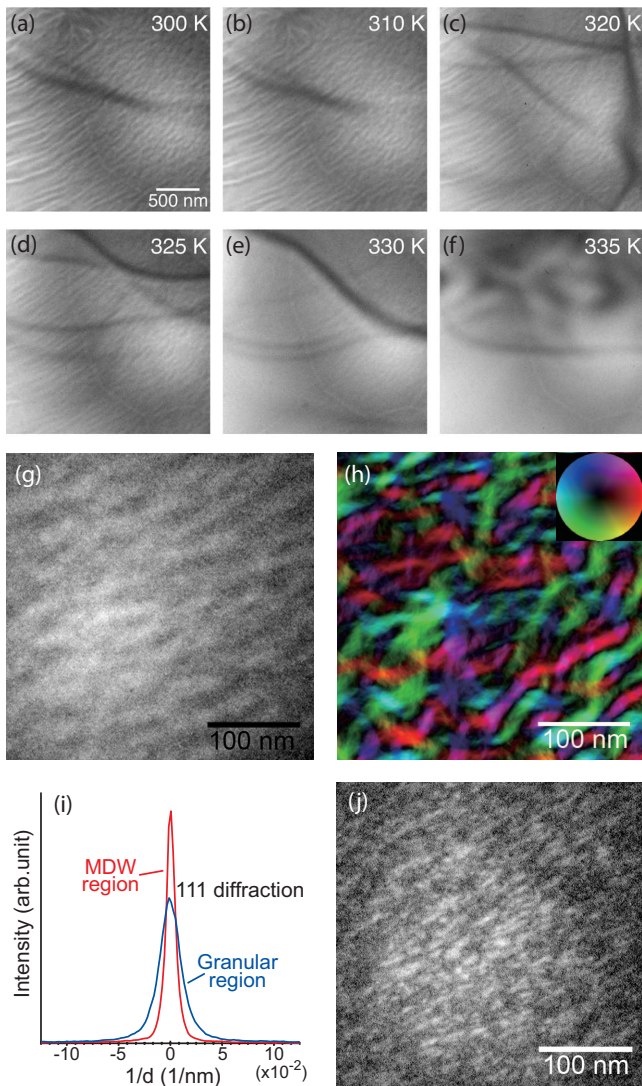

FIG. 5. (Color). (a)–(f) Temperature profiles of Fresnel images. (g) Magnified image of granular part in Fresnel image at 300 K. (h) TIE image corresponding to (g). The inset is a color wheel for interpretation of the color distribution map. (i) Intensity profiles of the 111 spots along $[1\bar{1}0]$. Red and blue lines represent the profiles for the regions where magnetic domain-wall images and granular contrast, respectively, appear. (j) Dark-field image formed with the 111 spot. This image was obtained from the same region as that shown in (g).

and l are odd numbers, for the granular contrast region were found to be significantly broader (about three times in FWHM) than those for the MDW contrast region, although the other diffraction spots have almost identical FWHMs. This indicates the regions where evolution of Fe/Mo ordering decreased to nanometer size. To verify this, we took DF images of the granular contrast region. Figure 5(j) shows the DF image formed with the 111 spot and the bright areas represent Fe/Mo-ordering domains. The DF image is completely different from the one of the MDW contrast region shown in Fig. 2(c), representing a granular structure with scattered droplets of less than 20 nm in diameter. We can recognize the dark lines in Fig. 5(j) as the densely developed APBs. The observed nanodroplets represent a short-range Fe/Mo ordering. Therefore the magnetic nanodomains (MNDs) are developed in the short-range Fe/Mo-ordering (SRO) region. The size of the MND was relatively larger than one of the SRO domain. This suggests that each MND was formed by conjunction of the magnetically correlated SRO domains. Development of such MNDs has been proposed in a doped system of the ordered double perovskites, $Sr_2Fe(W_{1-x}Mo_x)O_6$.[37] In the doped system, it has been suggested that the Fe-Mo clusters with the ferrimagnetic coupling were isolated from each other by the antiferromagnetic Fe-W domain and consequently that the ferromagnetic miniclusters, i.e., MNDs, are formed in the low-x compounds. The observed MND might have been formed by restriction of the coherent magnetic ordered region due to crystallographic SRO and resultant dense distribution of antiferromagnetic coupling on APBs.

IV. SUMMARY

We have investigated the relations between magnetic domain and antiphase domain structures in Ba_2FeMoO_6 by means of transmission electron microscopy. By direct observations of the magnetic domain and antiphase domain structures and the *in situ* Lorentz transmission electron microscopy observation as a function of external magnetic field, we proved that the magnetic domain walls were pinned at the antiphase boundaries due to their strong microscopic coupling—perhaps the antiferromagnetic coupling across the antiphase boundary. Furthermore, we have observed a magnetic nanodomain structure in the region where Fe/Mo ordering remains short-ranged. In the ordered double perovskites therefore the magnetic nanodomain structures may be possibly fabricated by controlling the crystallographic antiphase domain structures and the degree of crystallographic

[1] K.-I. Kobayashi, T. Kimura, H. Sawada, K. Terakura, and Y. Tokura, Nature (London) **395**, 677 (1998).

[2] F. S. Galasso, *Structure, Properties and Preparation of Perovskite-Type Compounds* (Pergamon, Oxford, 1969).

[3] A. W. Sleight and J. F. Weiher, J. Phys. Chem. Solids **33**, 679 (1972).

[4] Y. Tomioka, T. Okuda, Y. Okimoto, R. Kumai, K.-I. Kobayashi, and Y. Tokura, Phys. Rev. B **61**, 422 (2000).

[5] J. Gopalakrishnan, A. Chattopadhyay, S. B. Ogale, T. Venkatesan, R. L. Greene, A. J. Millis, K. Ramesha, B. Hannoyer, and G. Marest, Phys. Rev. B **62**, 9538 (2000).

[6] J. Lindén, T. Yamamoto, M. Karppinen, H. Yamauchi, and T. Pietari, Appl. Phys. Lett. **76**, 2925 (2000).

[7] J. M. Greneche, M. Venkatesan, R. Suryanarayanan, and J. M. D. Coey, Phys. Rev. B **63**, 174403 (2001).

[8] L. Balcells, J. Navarro, M. Bibes, A. Roig, B. Martínez, and J. Fontcuberta, Appl. Phys. Lett. **78**, 781 (2001).

[9] S. Colis, D. Stoeffler, C. Mény, T. Fix, C. Leuvrey, G. Pourroy, A. Dinia, and P. Panissod, J. Appl. Phys. **98**, 033905 (2005).

[10] C. Ritter, M. R. Ibarra, L. Morellon, J. Blasco, J. García, and J. M. D. Teresa, J. Phys.: Condens. Matter **12**, 8295 (2000).

[11] D. Sánchez, J. A. Alonso, M. García-Hernández, M. J. Martínez-Lope, J. L. Martínez, and A. Mellergård, Phys. Rev. B **65**, 104426 (2002).

[12] C. Kapusta, P. C. Riedi, D. Zajac, M. Sikora, J. M. D. Teresa, L. Morellon, and M. R. Ibarra, J. Magn. Magn. Mater. **242-245**, 701 (2002).

[13] M. Besse, V. Cros, A. Barthélémy, H. Jaffrès, J. Vogel, F. Petroff, A. Mirone, A. Tagliaferri, P. Bencok, P. Decorse, P. Berthet, Z. Szotek, W. M. Temmerman, S. S. Dhesi, N. B. Brookes, A. Rogalev, and A. Fert, Europhys. Lett. **60**, 608 (2002).

[14] D. Serrate, J. M. D. Teresa, and M. R. Ibarra, J. Phys.: Condens. Matter **19**, 023201 (2007).

[15] B. Martínez, J. Navarro, L. Balcells, and J. Fontcuberta, J. Phys.: Condens. Matter **12**, 10515 (2000).

[16] A. S. Ogale, S. B. Ogale, R. Ramesh, and T. Venkatesan, Appl. Phys. Lett. **75**, 537 (1999).

[17] L. Berger, Y. Labaye, and J. M. D. Coey, J. Magn. Magn. Mater. **242-245**, 1221 (2002).

[18] H. Q. Yin, J.-S. Zhou, R. Dass, J.-P. Zhou, J. T. McDevitt, and J. B. Goodenough, J. Appl. Phys. **87**, 6761 (2000).

[19] J. B. Goodenough and R. I. Dass, Int. J. Inorg. Mater. **2**, 3 (2000).

[20] J. Lindén, M. Karppinen, T. Shimada, Y. Yasukawa, and H. Yamauchi, Phys. Rev. B **68**, 174415 (2003).

[21] J. Navarro, L. Balcells, F. Sandiumenge, M. Bibes, A. Roig, B. Martínez, and J. Foutcuberta, J. Phys.: Condens. Matter **13**, 8431 (2001).

[22] T.-T. Fang, Phys. Rev. B **71**, 064401 (2005).

[23] X. Z. Yu, T. Asaka, Y. Tomioka, C. Tsuruta, T. Nagai, K. Kimoto, Y. Kaneko, Y. Tokura, and Y. Matsui, J. Electron Microsc. **54**, 61 (2005).

[24] S. B. Kim, B. W. Lee, and C. S. Kim, J. Magn. Magn. Mater. **242-245**, 747 (2002).

[25] O. Chmaissem, B. Dabrowski, S. Kolesnik, S. Short, and J. D. Jorgensen, Phys. Rev. B **71**, 174421 (2005).

[26] Recently, Ref. 25 reported that Ba_2FeMoO_6 below T_C has a tetragonal structure. However, we could not observe in our TEM observation the experimental evidence of tetragonal structure, such as significant change in lattice parameters and twin structure due to tetragonal distortion. We could not distinguish each crystal axis ($a \sim c$). Therefore to facilitate comparison between MDW and APB, we treated the crystal structure as a cubic $Fm\bar{3}m$ structure.

[27] K. Ishizuka and B. Allman, J. Electron Microsc. **54**, 191 (2005).

[28] M. R. Teaque, J. Opt. Soc. Am. **73**, 1434 (1983).

[29] K. A. Nugent, T. E. Gureyev, D. F. Cookson, D. Paganin, and Z. Barnea, Phys. Rev. Lett. **77**, 2961 (1996).

[30] V. V. Volkov and Y. Zhu, Phys. Rev. Lett. **91**, 043904 (2003).

[31] H. Zijlstra and H. B. Haanstra, J. Appl. Phys. **37**, 2853 (1966).

[32] A. J. Lapworth and J. P. Jakubovics, Philos. Mag. **29**, 253 (1974).

[33] Y. Murakami, H. S. Park, J. H. Yoo, D. Shindo, K. Oikawa, R. Kaimura, and K. Ishida, Met. Mater. Int. **10**, 207 (2004).

[34] D. T. Margulies, F. T. Parker, M. L. Rudee, F. E. Spada, J. N. Chapman, P. R. Aitchison, and A. E. Berkowitz, Phys. Rev. Lett. **79**, 5162 (1997).

[35] R. H. Wade, Proc. Phys. Soc. **79**, 1237 (1962).

[36] V. V. Volkov and Y. Zhu, J. Appl. Phys. **85**, 3254 (1999).

[37] K.-I. Kobayashi, T. Okuda, H. Tomioka, T. Kimura, and Y. Tokura, J. Magn. Magn. Mater. **218**, 17 (2000).